24 th EUROPEAN ROTORCRAFT FORUM
Marseilles, France - 15th-17th September 1998

SM03

ECD-0086-98-PUB

Examples for the Nonlinear Finite Element Analysis of Light Weight Helicopter Structures Using the FEM Code MARC

Peter Gergely
EUROCOPTER DEUTSCHLAND GmbH
81663 Munich, Germany

Weight saving aspects for structural aircraft parts are important basic requirements, often leading to a light weight design for thin walled shell structures. For these parts a Nonlinear Finite Element Analysis has to be conducted due to the geometrically nonlinear - and/or elastic-plastic material behaviour of these components. For this analysis, validated numerical tools like the FEM code MARC or other specialized software can be used with good reliability, taking into account large displacements and rotations (ε^2 terms). For this nonlinear analysis two examples will be presented here.

The first one is an example for geometric nonlinearity, and deals with the investigation of the buckling behaviour of a cylindrical shell made of carbon fiber composites, which is loaded by simultaneous bending moments at both cylinder ends. This work was carried out within the *framework of the European Brite-Euram* Project DEVILS, which means the Design and Validation of Imperfection-Tolerant Laminated Shells. These investigations can be applied for the design of a new composite tailboom structure for an advanced helicopter.

The second example shows a nonlinear analysis using the FEM code MARC for a bellow-shaped spring, which is successfully used as part of a vibration isolation element of the EC135 helicopter's ARIS-system (Anti Resonance Isolation System). This element is loaded simultaneously by axial tension and compression loads as well as internal pressure.

TABLE OF CONTENTS

1. OBJECTIVES

For rotorcrafts as well as fixed wing aircrafts weight saving aspects are very important. This is a basic requirement which is particularly true for helicopter structures.

Reducing the weight of these structures by using less wall thicknesses for isotropic shells or using composite shells with orthotropic material behaviour can be a solution for the design. Thus, for type certification of these light weight shell structures - apart from stiffness as well as static and fatigue strength requirements - also stability aspects become important. If possible, the buckling of structural shells should be avoided for all load combinations. This has to be shown by buckling tests and/or analysis.

Due to the fact, that full-scale buckling tests are expensive, the knowledge of the stability behaviour of the structure and the estimation of the buckling loads becomes more important in the stage of the design phase.

At this stage, all parameters who can contribute to the strength and stability behaviour of the real composite structure should be taken into account.

These parameters had been given in Ref. [5] and [8] within the framework of the European Brite-Euram Project DEVILS, which means the Design and Validation of Imperfection-Tolerant Laminated Shell Structures. These investigations can be applied in a later step for the design of *a new composite tailboom structure* for an advanced helicopter.

A new design philosophy for composite structures was realized first for the EC135 helicopter, Eurocopter's new twin-engined multi-purpose light helicopter , see Fig. 1.

Fig.1: The twin-engined multi-purpose light helicopter EC135.

As a modern helicopter, the EC135 offers state-of-the-art safety features like crashworthiness and damage tolerant layout and takes advantage of the latest design technology.

One of the major factors contributing significantly to the overall performance of the helicopter are advanced design features and materials. This includes the dynamic system as well as the fuselage. Weight saving, reduction of operating costs and improved performance are the benefits of incorporating advanced technology in the design.
The structure is designed to meet the latest certification requirements according to JAR27. These certification requirements also ask for some new specific characteristics concerning structure related safety aspects such as damage tolerance and crashworthiness. To ensure safe operation of the helicopter throughout its lifetime the primary structure has been designed taking into account damage tolerance criteria. This has been considered in the design process for example by using multiple load paths as well as by taking into account the presence of certain structural defects like impacts or manufacturing defects in composite parts or initial flaws in metallic parts when performing the dimensioning and lifetime calculations.

This means for example for the composite parts of a helicopter fuselage primary structure, that the design philosophy with respect to fatigue is to be based on the no-growth approach for present allowable manufacturing and non-visible in-service defects (minimum barely visible impact damages, BVID's), see Ref. [2] and Ref. [5].

The no-growth approach for composite parts takes advantage from the unique characteristics of composite materials that present defects don't grow under fatigue loading if a certain strain limit is not exceeded.
Furthermore, as there is no defect growth, the structure needs to have ultimate load capability for its complete service life.

Other important parameters for the design and evaluation of composite structures are the material data or the elastic constants of the laminate, as like Young's moduli, shear moduli, and Poissons ratios.
Due to the orthotropic behaviour of fiber reinforced plastics, for the general 3 dimensional case, 9 of these elastic constants have to be determined.

$$E_{11}, E_{22}, E_{33}, G_{12}, G_{23}, G_{13}, \nu_{12}, \nu_{23}, \nu_{13}$$

These elastic constants are important basic values for all composite structures. Due to the scatter of these values, a statistical approach should be used, to determine design values of these constants, corresponding to defined statistical probabilities as well as confidence levels (e.g. A- or B-values).

According to the MIL-HDBK-5, and the MIL-HDBK-17 - valid specially for composites - see Ref. [13], and the german LTF 9330-302 as given in Ref. [14], two commonly used statistical values are specified:

- A - values , which correspond to a statistical probability of 99 % , with a confidence level of 95 %
- B - values , which correspond to a statistical probability of 90 % , with a confidence level of 95 %

As design values for the composite's material data B - values could be used (redundant structures with different load-carrying members) .
This B-value means, that 90 % of all composite parts produced out of this material will have at least this design value or even higher, with a confidence of 95 %.

The use of B-values according to FAR 27.613 and JAR 27.613 for structural composite parts designed with respect to stiffness and strength as well as to buckling requirements, is based on experiences for the development of composite parts at ECD for long years.

For the material data also the air humidity and the surrounding temperature have to be considered in the stage of the design phase. This is important for the use of the resin-system for the composite part.

But, before these design requirements with respect to material data, stiffnesses, strain levels, stability aspects etc. could be realized for full-scale composite structures - like a composite tailboom structure for an advanced helicopter for example - reliable numerical tools have to be developed in order to predict the buckling behaviour of these real structural parts. For these structural components also different kinds of imperfections like geometric ones or different kinds of laminate defficiencies should be taken into account.
For the design and evaluation of light weight shell structures made of monolithic composites, at first, the validation of numerical tools for the buckling analysis of these structures has to be shown. For this task at first the buckling investigations have to be started with the case of simple composite cylindrical shells without any kind of imperfections, that is for ideal cylinders.

For these simplified cases of cylindrical shells, buckling tests are available. Thus, in a first step, the reliability of the buckling behaviour prediction (calculation of buckling loads and the corresponding buckling modes) has to be shown for these simple cases.
For this estimation, validated numerical tools like the FEM codes ABAQUS, NASTRAN and MARC, or other specialized software can be used with more or less reliability. For these light weighted aircraft structures often large displacements have to be considered and thus, the nonlinear capability of these FEM codes becomes more and more important.
For this nonlinear analysis two examples will be presented here, both of which have been conducted at Eurocopter Deutschland GmbH (ECD).

The first one is an example for the case of geometric nonlinearities, and deals with the investigation of the buckling behaviour of a cylindrical shell made of carbon fiber composites, which is loaded by simultaneous bending moments at both cylinder ends. This work was carried out under the above mentioned European Brite-Euram Project DEVILS .

The second example shows a nonlinear analysis using the FEM code MARC for the case of material nonlinearities. Here, the elastic/plastic material behaviour was taken into account for a thin walled bellow-shaped spring, which is successfully used as part of a vibration isolation element of the EC135 helicopter's ARIS-system (Anti Resonance Isolation System).
The four ARIS elements of the EC135 helicopter also deal as transmission Z-struts , and have to transmit the main rotor loads into the fuselage structure.
The bellow shaped spring elements of these ARIS components are loaded simultaneously by axial tension and compression loads as well as pressure loading.

The analysis for the material nonlinearity was based on the Ramberg-Osgood theory.
The numerical results for axial stiffness, strains and stresses can be validated by comparison with test results.
Both components of this ARIS system - the primary and secondary bellow shaped springs - had been analysed using the nonlinear capability of the MARC code.

2. BUCKLING ANALYSIS OF A COMPOSITE CYLINDRICAL SHELL LOADED BY END BENDING MOMENTS

This work was conducted within the framework of the BRITE-EURAM PROJECT **DEVILS**, which means the **D**esign and **V**alidation of **I**mperfection-**T**olerant **L**aminated **S**hell Structures. (see Ref. [1]).

One basic target of this project was the evaluation of reliable numerical tools for the prediction of the buckling behaviour for different isotropic or orthotropic cylindrical shells for different loading cases. These investigations for simple load cases and geometrically ideal cylinders should allow the buckling analysis for real composite tailboom structures which have to sustain different combinations of landing- and flight loads (bending and torsional moments as well as lateral and axial loads acting simultaneously).
Due to the fact, that the FEM code MARC was used successfully at ECD for long years and has shown a high reliability for geometric and material nonlinear problems (analysis of viscoelastic behaviour of elastomeric bearings and dampers etc.), ECD has decided to use MARC also for the nonlinear buckling analysis problems as specified in the Brite Euram Project DEVILS.

Thus, one subtask of this project was the investigation of the buckling behaviour for an ideal composite cylinder without any kind of imperfections. This cylinder should be loaded by bending moments acting simultaneously at both cylinder ends. As boundary condition it was assumed, that the initial radius at both cylinder ends had to be maintained for all load increments.
The first 3 buckling loads as well as buckling modes were determined by means of a nonlinear analysis using the FEM-code MARC.

The numerical results as given in Ref. [6], were compared with test results as given in Ref. [9], showing a good correlation.
Due to this correlation between the presented results of the buckling tests and the numerical results determined by the MARC analysis, the reliability of the numerical tools implemented in MARC could be shown.

At the beginning, some theoretical considerations will be given in the following chapter. These basic concepts should contribute to a better understanding of the stability behaviour of shell structural parts.

2.1 Basic Considerations for the Stability of Shells

It is beyond the scope of this paper to present details of the theory for the stability of isotropic and orthotropic shells. For these detailed informations the corresponding literature should be used.
Here only an overview about various shell buckling phenomena shall be given, based on two references according to [3] and [8] . Thus, this chapter should also represent an effective introduction to our buckling problem for the composite cylinder loaded by end bending moments.

A structure may lose its stability mainly in two ways, namely by snap-through - and bifurcation behaviour.
The snap-through (or limit point) instability is characterized by decreasing stiffness of the structure with increasing load. The equilibrium path is stable until the maximum value of the load, called limit load P_L of the structure is reached, see Fig. 2 bellow.

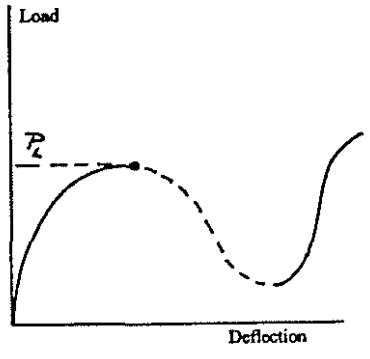

Fig.2: The snap-through (or limit point) instability, see Ref. [8].

At this point, the path becomes unstable and the structure buckles in an instantaneous manner. A dynamic jump occurs before the structure comes to rest on an other stable equilibrium path. During this jump, the structure has undergone large deformations.
Laterally loaded arches and domes are examples for snap-through behaviour. For this kind of buckling behaviour, a non-linear response occurs, before the limit load is reached. Thus a non-linear prebuckling of the structure has to be considered.

Bifurcation instability takes place when 2 or more equilibrium paths goes through the same point. The fundamental (or pre-buckling) equilibrium path is intersected by the secondary (or post-buckling) path at the bifurcation point. The corresponding load at this point is called the critical load P_{cr}, see Fig. 3 bellow. The pre-buckling path is stable up to this critical load and can be stable or unstable beyond it. This depends on the type of bifurcation.
Along the post-buckling path the deformations begin to grow in a new pattern, called the buckling mode, which is quite different from the fundamental deformation pattern.
(pre-buckling pattern).

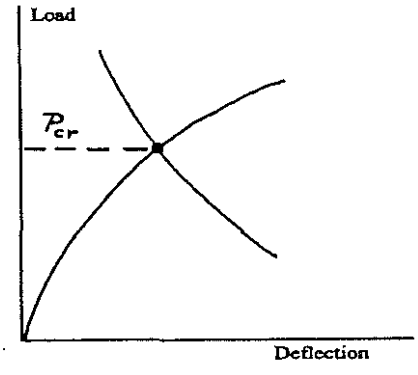

Fig.3: The bifurcation instability, see [8].

Considering load deflection diagrams in which the x-axis represents the amplitude of the buckling mode displacement called w_0, see Fig. 4 , asymmetric, stable symmetric and unstable symmetric bifurcation types can be distinguished.

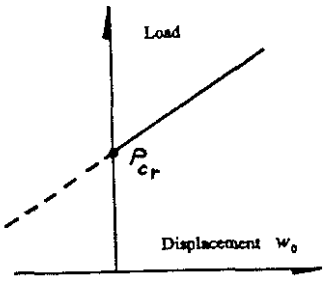

(a) Asymmetric bifurcation

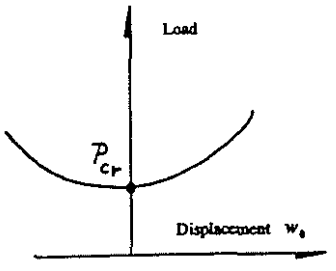

(b) Stable symmetric bifurcation

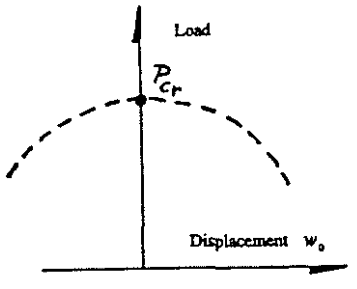

(c) Unstable symmetric bifurcation

Fig.4: Different types of bifurcation instability, see [8], solid lines represent stable paths, dashed lines represent unstable paths.

Asymmetric bifurcation is rare in comparison with symmetric bifurcation. One example for this rare type of bifurcations are eccentrically loaded rigid-jointed frames.
Stable symmetric bifurcation occurs for plates under in-plane loading, whereas a large amount of shell buckling problems yield unstable symmetric bifurcations.

A very difficult instability problem occurs for the case of compound bifurcations, where several buckling modes are associated with the same critical load. The axially compressed cylinder and the externally pressurised sphere are well known classical examples for this kind of stability problems. Here, the post-buckling behaviour is affected by non-linear interaction of the buckling modes.
For some shell problems - mainly axisymmetrically loaded shells of revolution - the prebuckling nonlinearity has a significant effect on the value of the critical load and on the shape of the buckling mode. For these cases a nonlinear eigenvalue analysis is required to find the bifurcation point on the prebuckling path, and thus to predict the critical load and buckling mode.
Fig. 5 taken from Ref. [8] , shows a spherical cap under external pressure, where both snap-through and bifurcation instabilities can occur. This behaviour shown in Fig. 5 is typical for pressurised spherical caps within a particular range of the shallowness parameter (h / H) . If this parameter value changes, the stability behaviour also changes significantly.

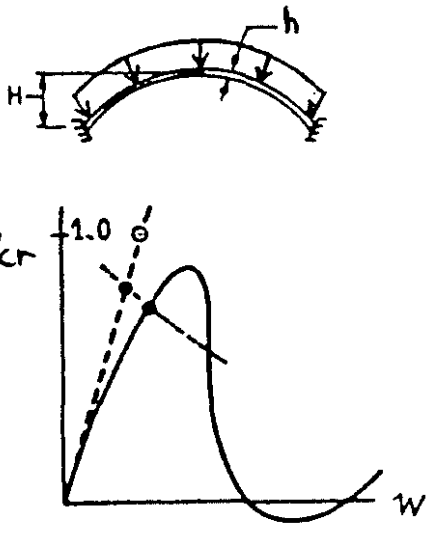

- Complete Spherical Shell Bifurcation Buckling Pressure
- Spherical Cap Bifurcation Pressure

Fig.5: Spherical cap under external pressure, load deflection diagram taken from Ref. [8]
– – – – Linear Prebuckling
——— Nonlinear Prebuckling

2.2 Theoretical Investigations

Some basic theoretical considerations for transverse loaded cylindrical shells with different geometries had been published in Ref. [3].
This work was conducted in the year 1973 at the "Deutsche Forschungs- und Versuchsanstalt für Luft- und Raumfahrt", (DFVLR).

Additionally, the theoretical considerations can be based on Ref. [4], which gives a very good survey about all theoretical aspects of buckling for different loadcases and their combinations. This reference gives also an approach to estimate the buckling loads for conical shells.
Compared to the classical stability problems of cylindrical shells - the buckling problems under axial compression load and outer pressure - the stability problem for a cylindrical shell clamped to a wall at one end and loaded by a transverse load at the other free end, was not often investigated.
A reason for this had been numerical difficulties to solve the differential equations of this problem, and the lack of reliable numerical tools in the past.

For special cases, the assumption of a membrane stress condition before buckling occur can be postulated for classical stability problems. These membrane stresses can be assumed to be constant in the cylinder's longitudinal - and circumferencial direction. The stress distributions in the shell before buckling can occur are called often "basic stress conditions".
The exact solutions of the governing differential equations for these basic stress conditions are known to be periodic functions for the buckling modes, see Ref. [3].

These assumptions are not valid for our buckling problem for a cylindrical shell loaded by pure bending moments (two simultaneous end moments). For this case, the basic stress condition is only constant in longitudinal, but not constant in circumferencial direction. Thus, the corresponding buckling modes for this loadcase are only periodic in the longitudinal cylinder direction. In circumferential direction, the radial cylinder displacements are strongly located, see Ref. [3] and [9]. Exact solutions of the governing equations are not known for this case. Thus, a finite elemente analysis or other specialised numerical methods should be used.

For the case of a transverse loaded cylinder as shown in Fig. 6, both, the direct and shear stresses for the basic stress condition (fundamental or prebuckling equilibrium path) are not constant in both directions. Thus, the corresponding buckling modes are not periodic in the longitudinal as well as the circumferential cylinder direction.
At the point on the circumference of the cylinder, where the maximum value of the direct stress occurs, the shear stresses are zero, see point P1 in Fig. 6. This apply also for the shear stresses in changed sense.

$$N_{x_0} = -\frac{Q * L}{\pi * R^2} * \frac{x}{L} * \cos\frac{y}{R}$$

$$N_{xy_0} = \frac{Q}{\pi * R} * \sin\frac{y}{R}$$

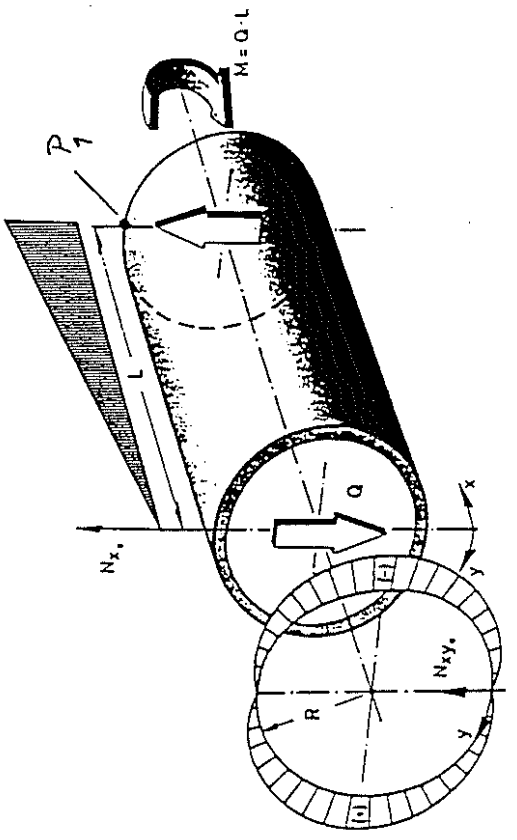

Fig. 6 : Fundamental stress condition for the transverse loaded cylinder (taken from Ref. [3]).

The ratio between these maximum stresses depends on the radius to length ratio R / L of the cylinder.
The loss of stability can occur in two basic buckling modes:

1. if the max. shear stresses in the neutral plane are reaching a critical value (see Fig. 6), or

2. if the direct stresses in point P1 (fixing to the wall) in Fig. 6 are reaching a critical value .

This means, that for short cylinders - low ratios of L/R - mainly the shear stresses will contribute to buckling, and for long cylinders - L/R higher - the influence of the direct stresses on the buckling behaviour of the cylinder are increasing.

Buckling tests with cylinders as given in Ref. [3], have shown, that the loss of stability is caused for long cylinders mainly by buckling modes due to bending. Here the influence of the direct stresses is higher. The buckling modes observed in buckling tests have shown the following distribution :

1. the buckling modes are distributed at the cylinder's bottom surface, only over a small local region in the circumferencial direction,

2. the buckling modes are evanescent in the cylinder's longitudinal direction from the clamped end, were the direct stresses have maximum values to the loaded cylinder end , (see Fig. 6) .

It is very difficult to find out the buckling modes for these kind of cylinders, that means, to calculate all the configurations which lead to a minimum of the buckling load. Exact solutions of the governing differential equations are not known, and thus, numerical tools like the FEM code MARC must be used. This work has been conducted in Ref. [6] also within the Brite Euram Project DEVILS.
The calculated buckling loads compared with the test results have shown the reliability of the numerical tools implemented in the MARC FEM-code.

2.3 Nonlinear Analysis with the FEM code MARC

MARC can be used for extremely nonlinear problems and allows automatic load stepping in a quasistatic fashion for geometric large displacements. This is done by MARC with the AUTO INCREMENT option, which can handle snap-through phenomena as well as the postbuckling behavior of structures.
Both, a linear as well as a nonlinear analysis can be conducted. The program determines at what load the structure will collapse. This buckling of the structure is detected at the point where the structere's stiffness matrix approaches a singular value.

2.3.1 Basic numerical tools

The following incremental approach for buckling analysis is used in all FEM codes like MARC or others:

A) Linear Buckling (without LARGE DISP)

Eigenvalue analysis solving the following equation:

$$\left\{K_L + \lambda * K_\sigma\right\} * u = 0$$

where, K_L = linear stiffness matrix (ε - terms)
K_σ = stress stiffness matrix
λ = eigenvalue obtained by the inverse power sweep or the Lanczos method.

B) Nonlinear Buckling (with LARGE DISP)

Eigenvalue analysis solving the equation:

$$\left\{K_\sigma + K_L + K_{nl} + \lambda * K_{\Delta\sigma}\right\} * u = 0$$

where, the following additional terms have to be considered

K_{nl} = geometric stiffness matrix (ε^2 - terms)
$K_{\Delta\sigma}$ = incremental stress stiffness matrix ($\Delta\sigma$)

For the solution two different cases have to be distinguished:

(1) No Recycling in last increment :

$$K = K_\sigma + K_L + K_{nl}$$

$$\Rightarrow \quad \lambda = \lambda^*$$

(2) Recycling in last increment :

$$K = K_{\sigma+\Delta\sigma} + K_L + K_{nl}$$

$$= K_\sigma + K_L + K_{nl} + K_{\Delta\sigma}$$

$$\Rightarrow \quad \lambda = \lambda^* + 1$$

Buckling Load (Solution)

$$P_{Buckling} = P_0 + \lambda * \Delta P \qquad \text{with}$$

$P_0 =$ Load up to previous increment

$\Delta P =$ Load in previous increment

In MARC two different numerical tools are implemented in order to solve the eigenvalue problem. The inverse power sweep and the Lanczos methods, which can be used alternatively. Here a short description will be given, how the Lanzcos method works.

The Lanczos algorithm implemented in the FEM-code MARC converts the original Generalized Eigenvalue Problem into the determination of the eigenvalues of **tri-diagonal symmetric positive definite matrices.**
Using the Lanczos solver, MARC conducts the determination of all or a small number of modes.
For a small number of modes, this Lanczos method is the most efficient and powerful eigenvalue extraction algorithm.
The user can be sure, to get the minimum eigenvalue corresponding to the minimum buckling load, because all eigenvalues and modes are sorted for the output post file.

⇒ **Generalized Eigenvalue Problem**

$$K_L * u + \lambda * K_\sigma * u = 0 \qquad \Leftrightarrow$$
$$\{A * x = \lambda * B * x\}$$

$$\frac{1}{\lambda} * K_\sigma * u = -K_\sigma K^{-1} K_\sigma u$$

Transformation matrix Q

$$u = Q * \eta \qquad \Rightarrow$$

$$\frac{1}{\lambda} * K_\sigma * Q * \eta = -K_\sigma K^{-1} K_\sigma Q \eta \qquad / \bullet Q^T$$

$$\frac{1}{\lambda} * Q^T K_\sigma Q \eta = -Q^T K_\sigma K^{-1} K_\sigma Q \eta$$

with the Unit Matrix: $Q^T * K_\sigma * Q = 1$

and the symmetric
tri-diagonal matrix T: $Q^T K_\sigma K^{-1} K_\sigma Q = T$

⇒ **New Eigenvalue Problem**

$$\frac{1}{\lambda} * \eta = -T * \eta \qquad \leftrightarrow$$
$$\langle A * x = \lambda * x \rangle$$

Selective orthogonalization of Lanczos vectors is conducted, and the determination of the eigenvalues is carried out by means of the **standard TQL-method** (characteristic polynomial method).

⇒ **Non Positive Definite Stress Stiffness Matrix**

The K_σ not positive definite eigenvalues cannot be calculated directly. The solution implemented in MARC uses an approach to solve this problem indirectly by means of the following approach:

$$K_L * u + \lambda * (K_\sigma + K_L) * u - \lambda * K_L * u = 0$$
$$(1 - \lambda) * K_L * u + \lambda * (K_\sigma + K_L) * u = 0$$

$$K_L * u + \frac{\lambda}{1 - \lambda} * (K_\sigma + K_L) * u = 0$$

reduces to the solution of the tensor equation:

$$K_L \bullet u + \lambda^* \bullet (K_\sigma + K_L) \bullet u = 0$$

with: $$\lambda^* = \frac{\lambda}{1-\lambda}$$

$$\Downarrow$$

and thus: the solution $$\lambda = \lambda(\lambda^*)$$

There are different ways to control the convergence of the solution:

⇒ **Convergence Controls** (very important)

→ Maximum number of iterations
→ Difference between eigenvalues in two consecutive sweeps divided by the eigenvalue is less than the tolerance
→ Normalized difference between all eigenvalues satisfies the tolerance

→ Two steps :
1) Matrix-transformation and orthogonalization of vectors (this process is not iterative)
2) Characteristic polynomial method (this process is iterative).

2.3.2 Description of the FEM model

This analysis concerns the calculation of buckling loads of a symmetrically laminated composite cylinder fixed at both ends, under the action of simultaneous bending moments acting on both cylinder ends (see Ref. [6]).

Geometry

This composite cylinder considered for buckling analysis has the following geometric values, see Ref. [6]:

	geometric values
Length L:	L = 304 mm
Midsurface Radius R:	R = 152 mm
Wall Thickness:	t = 0.944 mm
Length / Radius Ratio	L/R = 2
Radius / Thickness Ratio:	R/t = 161

The cylinder is assumed to be perfect, exhibiting no initial imperfections.

Materials Properties

The cylinder is made of AS4/3502 graphite/epoxy prepreg tape, with a quasiisotropic stacking sequence of

$[-45, +45, 0, 90]_S$. Each ply is 0.118 mm thick and has the following material properties (Unidirectional Laminate values , 0°- degree ply):

$E_1 = 161.10$ Gpa
$E_2 = 12.10$ Gpa
$G_{12} = 7.10$ Gpa
$G_{23} = 3.55$ GPa
$G_{13} = 7.10$ GPa
$\nu_{12} = 0.285$

Here, the index 1 means parallel to the fiber, index 2 means perpendicular to the fiber and index 3 means perpendicular to the 1-2 plane.

Boundary Conditions

All structural nodes at both ends of the cylinder have all their 6 degrees of freedom free and are connected (tied) with rigid links to 2 additional non structural auxiliary nodes called here P1 at one cylinder end and P2 at the other end., located at the center of each end on the cylinder axis of symmetry. These auxiliary nodes P1 , P2 have been verified by the TYING 80 option of MARC.
Using TYING type 80 means, that each node P1 , P2 consists of 2 nodes A and B lying on the same geometrical point, but with different degrees of freedom for the analysis:

Retained Nodes P1 and P2 for Tying 80	Global Degree of Freedom
A (not loaded)	u, v, w - translations only
B (loaded by bending rotations in radians of angles)	px, py, pz - rotations only

Both nodes P1, P2 have all their degrees of freedom fixed, except their rotation about the x axis (x axis is normal to the cylinder axis of symmetry).
Thus, both ends remain flat and circular maintaining their initial radius, while they can both rotate about the transverse axis x of the cylinder.

Loading

The cylinder is loaded by applied rotations (in radians of angles) about the transverse x-axis, on both its ends. These bending rotations are applied on the auxiliary nodes P1 and P2 of each end, symmetrically with respect to the cylinder mid-length (z is the cylinder axis), (see Ref. [6]).

Thus, Node P1 located at z = 0 mm (x=y=0) see a rotation of

$$\delta_x [rad]$$

and Node P2 located at z = L = 304 mm (x=y=0) see a rotation of

$$-\delta_x [rad]$$

Analysis

Type of Elements

The composite cylinder was modelled using 4-node shell elements, accounting for transverse shear effects. This is possible by means of using MARC element 75 together with the TSHEAR option.

- Bilinear, four-node shell elements including transverse shear effects (MARC Element 75) and orthotropic material model varified by the ORTHOTROPIC option of MARC
- The symmetric laminate lay-up (stacking sequence), thickness of each layer and its fiber orientation angle, were defined by the COMPOSITE option of MARC for each element.

Finite Element Model

FEM-Mesh

As a coarse finite element model a mesh of 36 four-node shell elements Typ 75 in the longitudinal (z-direction along the cylinder axis) and 36 in the circumferential direction was used (this mesh was defined by the code C x L = 36 x 36 shell elements).
Comparing the test results with the predicted buckling loads derived with this coarse mesh, it was found, that a more refined mesh consisting of more elements should be investigated.

Thus, an FEM model, with 72 x 72 - elements, and also a very fine mesh with 100 x 100 - elements were also investigated, see Table 1.

Element type	Mesh C x L
Shell element type 75 laminate	36 x 36
Shell element type 75 laminate	72 x 72
Shell element type 75 laminate	100 x 100

Tab. 1 : Different FEM meshes for the composite cylinder (*coarse, medium and fine mesh*).

Type of Analysis

Following calculations have been performed successfully:

- Nonlinear buckling analysis (with large displacements) using the inverse power sweep method.
  This geometrical nonlinear calculation leads for each load-increment to a nonlinear step with respect to the stresses ($\Delta\sigma$ on page 7). This means for the power sweep solver, that the solution could converge.

- Nonlinear buckling analysis (with large displacements) using the Lanzcos method.
  The results are nearly the same compared to the corresponding ones evaluated with the inverse power sweep solver. With Lanzcos, the eigenvalues are calculated and printed in sorted forms. Thus, the user can be sure, to get the minimum buckling load, which is of course of technical interest.

2.3.3 FEM results

The results of the nonlinear buckling analysis are summarized in Table 2 for all FEM-models for the first 6 (3 for mesh 72 x 72, one for mesh 100 x 100) eigenvalues. The associated mode shapes for the first 3 subincrements (the eigenmodes) will be reported for the best result (mesh 100 x 100), in Figures 7 to 11.

Mesh C x L	Mode No.	eigen-value λ	Buckling rotation MARC θ [rad]	Buckling End Moment **MARC-result** [kNm]
36 x 36	-	-	= λ * δx = λ * 0.0003	= λ * ΔM = λ * 1.30521
	1	13.677	0.004103	**17.85**
	2	13.698	0.004109	17.88
	3	14.259	0.004278	18.61
	4	14.335	0.004301	18.71
	5	15.287	0.004586	19.95
	6	15.389	0.004617	20.1
72 x 72	-	-	= λ * δx = λ * 0.0003	= λ * ΔM = λ * 1.311
	1	12.32	0.0037	**16.15**
	2	12.32	0.0037	16.15
	3	12.64	0.0038	16.57
100 x 100	-	-	= λ * δx = λ * 0.0003	= λ * ΔM = λ * 1.31206=
	1	12.11	0.0037	**15.89**

Tab. 2 : Results of the buckling analysis performed by MARC with different numerical models for several subincrements (called here modes).

Since the load $P_{beginning}$ at increment 0 (in the model definition of MARC) is zero, and the first load increment (load history definition of MARC) was defined with $\Delta\theta = 3*10^{-4}$ [rad] - simultaneous rotation acting on both cylinder ends - , the buckling end-rotations and buckling end-moments are given by the formula:

$$(\theta_{Buckle})_n = \lambda_n * \Delta\theta = \lambda_n * 3*10^{-4}[rad]$$

$$(M_{Buckle})_n = \lambda_n * \Delta M_0$$

ΔM_0 is the corresponding moment at the auxiliary non structural nodes P1 (or P2) at the x-rotation degree of freedom, calculated and given by MARC with the REAC option (reactions). This value corresponds to increment 1.

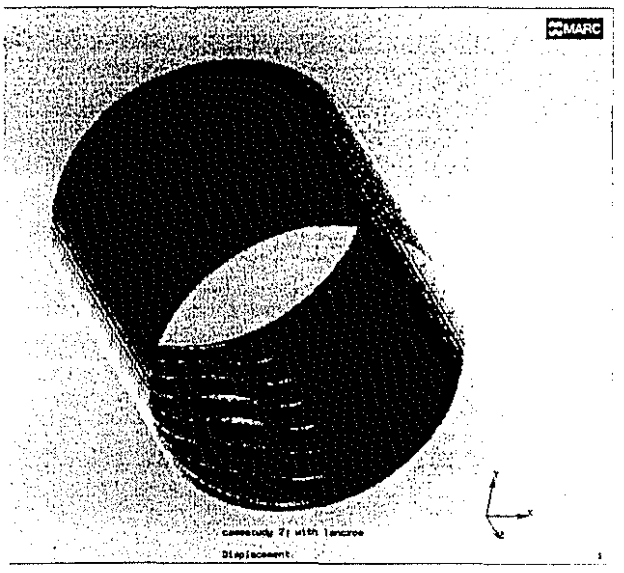

Fig. 7 : First buckling mode of the composite cylinder loaded by simultaneous end-moments (orthotropic shell, 100 x 100 elements), subincrement 1, perspective view.

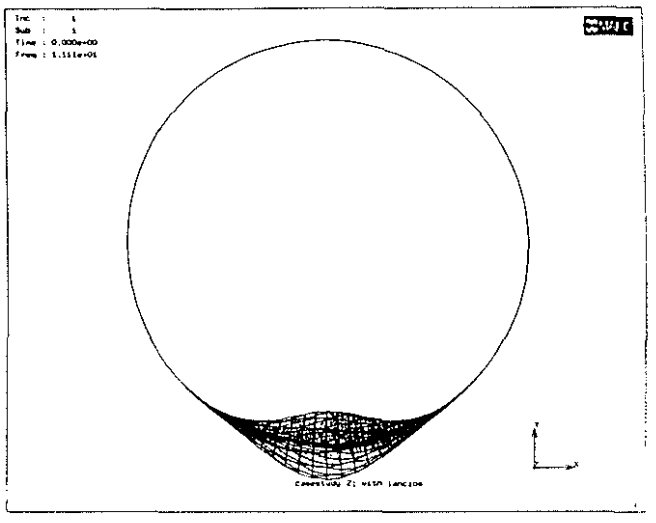

Fig. 8 : First buckling mode of the composite cylinder loaded by simultaneous end-moments (orthotropic shell, 100 x 100 elements), subincrement 1, view in z - direction, showing the total displacements (eigenvector).

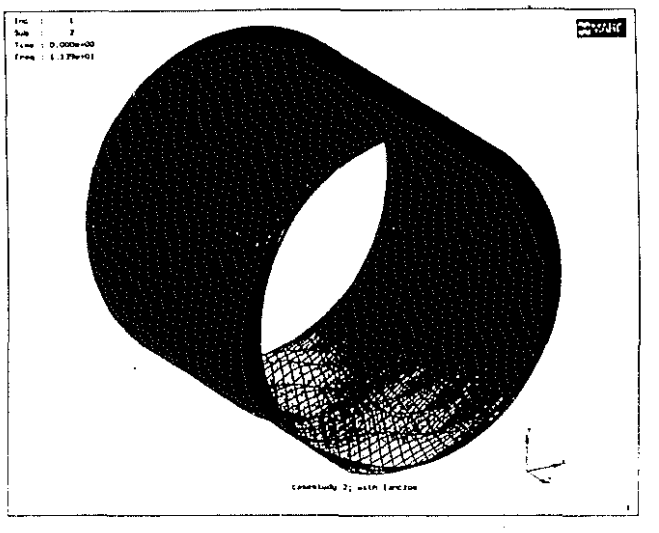

Fig. 10 : Second buckling mode of the composite cylinder loaded by simultaneous end-moments (orthotropic shell, 100 x 100 elements), subincrement 2 , perspective view

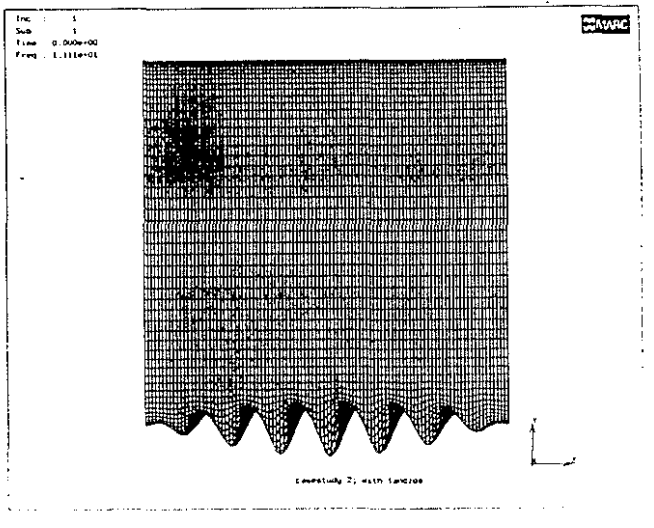

Fig. 9 : First buckling mode of the composite cylinder loaded by simultaneous end-moments (orthotropic shell, 100 x 100 elements), subincrement 1, view on y-z - plane, showing the total displacements (eigenvector).

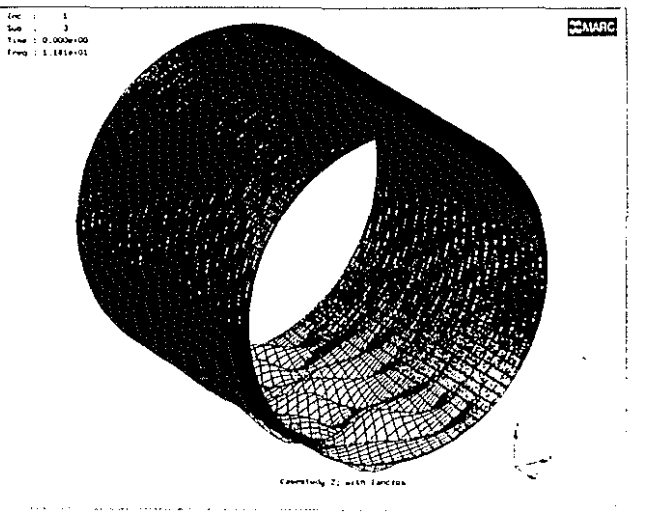

Fig. 11 : Third buckling mode of the composite cylinder loaded by simultaneous end-moments (orthotropic shell, 100 x 100 elements), subincrement 3 , perspective view

In the buckling analysis with MARC, not only the displacements, but also other important values, such as stresses and strains in each layer, the Mises stresses, the strain energy density etc. were determined writing all these values on a post tape.

As an example, the strain energy density for this buckling problem will be reported in Figure 12.
This important value, derived from the FEM calculation gives informations to a design egineer, that perhaps he should reinforce some regions with high strain energy density in the composite structure by means of additional layers (prepregs).

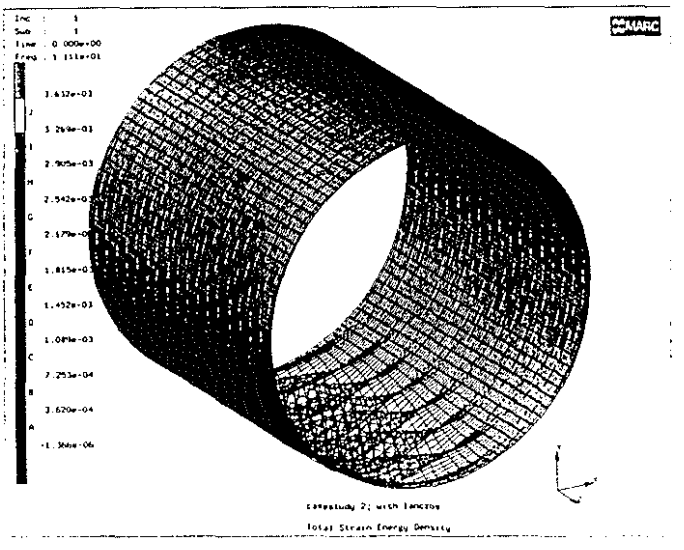

Fig. 12 : *Strain energy density of the composite cylinder* loaded by simultaneous end-moments (orthotropic shell, 100 x 100 elements), subincrement 1 , perspective view .

The equivalent von Mises stress of the composite cylinder loaded by simultaneous end-bending moments will be also reported in Figure 13.

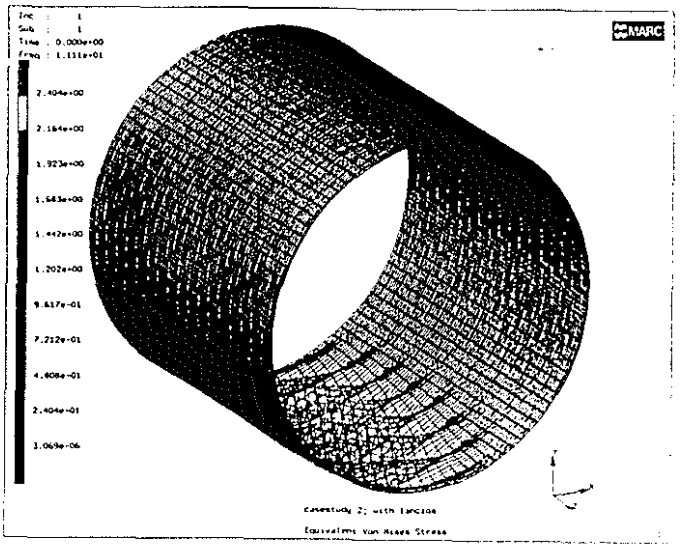

Fig. 13 : Equivalent von Mises stress of the composite cylinder loaded by simultaneous endmoments (orthotropic shell, 100 x 100 elements), subincrement 1 , perspective view .

2.4 Validation of the numerical tools by comparison with theory and test results

The composite cylinder as calculated in the last chapter , was tested according to Ref. [9], and the buckling end-rotations as well as the corresponding buckling end-moments had been determined.
In these buckling tests 5 eight-ply graphite-epoxy shells (see Table 3) with a length-to-radius ratio of L/R=2 and a radius-to-thickness ratio of approximately R/t=160 had been tested through loading rings as shown in Figure 14.

All these cylinders were made from the same material AS4/3502 . The material properties are exactly the same as for the calculated cylinder in chapter 2.3. Only the wall-thicknesses as shown in Table 3 show little difference. From Table 3 we can see, that the data of the tested cylinder named CYL-1A with t=0.95 mm (called H in this reference) is closest to our calculated shell of the last chapter .
Thus, the predicted buckling loads derived from the MARC-analysis can be compared with the test results for this shell named CYL-1A of the buckling tests as given in Ref. [9].

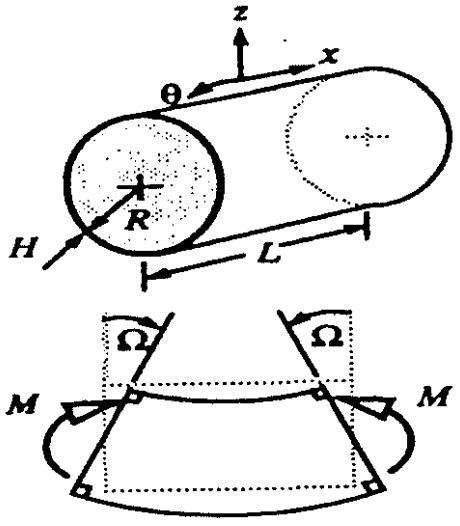

(a) Geometry and loading.

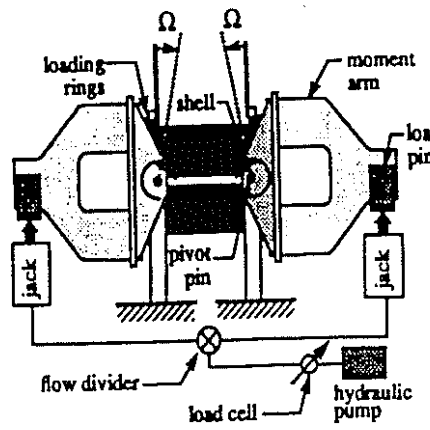

(b) Bending fixture schematic.

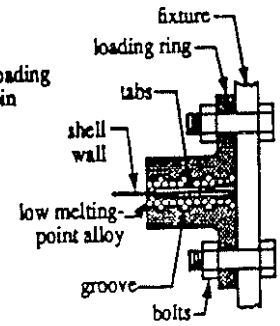

(c) Loading rings.

Fig. 14 : Test set-up for the buckling tests acc. to Ref. [9], shell geometry, loading, test fixture and loading rings, (Figure is taken from Ref. [9]).

Specimen	Layup	H, mm	$\frac{R}{H}$	M_{cr}, N-m	Ω_{cr}, degrees	ε_x^{cr}, με	$\frac{\lambda}{L}$	m
CYL-1A	$[\mp 45/0/90]_S$	0·950	160	15 630	0·207	3 610	0·067	15 0
CYL-1B	$[\mp 45/0/90]_S$	0·953	160	15 680	0·207	3 617	0·067	15·0
CYL-3A	$[\mp 45/0_2]_S$	0·968	156	10 731	0·098	1 697	0·083	12·0
CYL-4A	$[\mp 45/90_2]_S$	0·937	163	16 170	0·484	8 383	0·056	17·9
CYL-4B	$[\mp 45/90_2]_S$	0·909	167	15 714	0·465	8 114	0·055	18·2

Tab. 3 : Summary of the test specimens for the buckling tests, which were conducted acc. to Ref. [9].

In Ref. [9] also an FEM-calculation was carried out, and the predicted buckling loads were compared to the test results. Additionally a theoretical calculation was conducted, and the critical bending moment M_{CR} was calculated by means of the formula, as taken from Ref. [9]

$$M_{CR} = 2\pi R^* \sqrt{E_\theta H D_{11}} \quad , \text{ where}$$

D_{11} is the axial laminate bending stiffness

H = t is the shell wall thickness
R is the midsurface radius
E_θ is the smeared laminate circumferencial inplane stiffness

The number of axial halfwaves, m , of the corresponding axisymmetric buckling mode shape is acc. to Ref. [5]

$$\frac{m*\pi}{L} = \frac{\pi}{\lambda} = \left\{ \frac{D_{11}*R^2}{E_\theta * H} \right\}^{1/4} ,$$

where L is the shell length, and

λ is the half-wavelength of the mode shape.

All these theoretical values were computed in Ref. [9] and are given in Table 3.
Figure 15 shows the measured moment versus end-rotation responses for 3 representative cylinders. The bending moments and end-rotations in this figure were normalized by the classical buckling moment and end-rotation of the quasi-isotropic specimen CYL-1A, see Table 3. The prebuckling, buckling, and postbuckling responses are given in this Figure 15.

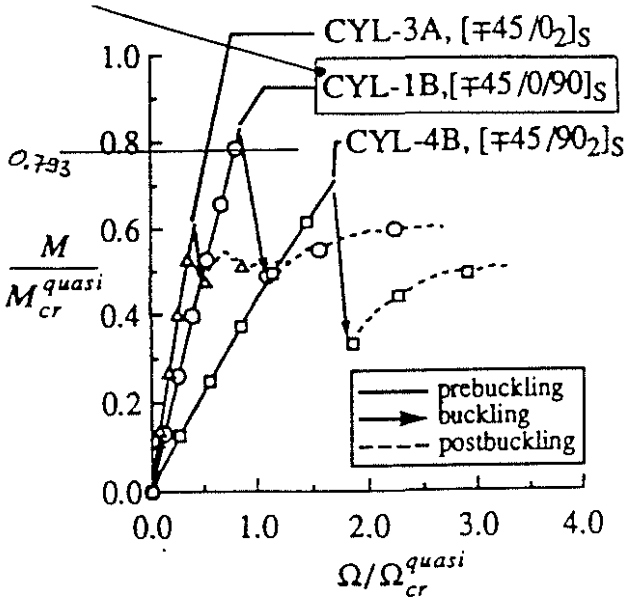

Fig. 15 : Measured bending moment versus end-rotation response for three specimens, (Figure is taken from Ref. [9]).

Table 4 gives a comparison of the finite element predictions and the experimental observations as derived in Ref. [5].

Specimen		Experiment			STAGS perfect shell		STAGS imperfect shell	
Specimen No.	Layup	M_{EXP}/M_{cr}	Ω_{EXP}/Ω_{cr}	No. of loadings	M^*_{FE} %	Ω^*_{FE} %	M^*_{FE} %	Ω^*_{FE} %
CYL-1A	$[\mp 45/0/90]_S$	0·793	0·831	2[b]	29·5	23·2	20·3	14·6
CYL-1B	$[\mp 45/0/90]_S$	0·852	0·877	3	19·8	16·5	7·9	4·9
CYL-3A	$[\mp 45/0_2]_S$	0·933	0·916	2[b]	16·2	17·9	14·9	16·3
CYL-4A	$[\mp 45/90_2]_S$	0·686	0·721	1	35·4	26·1	28·9	20·0
CYL-4B	$[\mp 45/90_2]_S$	0·734	0·775	1	28·7	19·4	6·9	1·0

a. $M^*_{FE} = (M_{FE} - M_{EXP})/M_{EXP} \times 100\%$ and $\Omega^*_{FE} = (\Omega_{FE} - \Omega_{EXP})/\Omega_{EXP} \times 100\%$. Finite element predictions and experimental observations are indicated by the subscripts 'FE' and 'EXP', respectively.
b. A reduction in buckling resistance was observed in the final loading.

Tab. 4 : Comparison of buckling values for 5 specimens of the buckling tests, which were conducted acc. to Ref. [9].

In Table 5 the buckling end moment values calculated with the FEM-code MARC for the coarse , the medium and the fine mesh are given in comparison with the theoretical value for this laminate lay-up and the test results as given in Ref. [9].

Mesh C x L	eigen-value λ MARC -result	Buckling End Moment MARC-result [kNm]	Buckling End Moment Theory [kNm]	Buckling End Moment Measured (*) [kNm]
36 x 36	-	= λ * ΔM = λ * 1.30521		
	13.677	**17.85**	**15.63**	**12.4**
	13.698	17.88	-	-
	14.259	18.61	-	-
72 x 72	-	= λ * ΔM = λ * 1.311		
	12.32	**16.15**	**15.63**	**12.4**
	12.32	16.15	-	-
	12.64	16.57	-	-
100 x 100	-	= λ * ΔM = λ * 1.31206= [KNM]		
	12.11	**15.89**	**15.63**	**12.4**

(*) Buckling Tests had been conducted at the NASA Langley Research Center in the United States.

Tab. 5 : Comparison of buckling values calculated by MARC with the theoretical value and the test results acc. to Ref. [9].

Comparing the predicted minimum buckling load determined through MARC's best result of **15.89 kNm** according to Table 5 above for the case of t = 0.944 mm wall-thickness, with the buckling load derived by the tests for CYL-1A with t = 0.95 mm of about 0.793*15.63 [kNm] = **12.4 kNm**, (see Tables 3 and 4), we get a difference between both values of about :

$$\Delta M_{Buckle}[\%] = \frac{M_{Marc} - M_{Test}}{M_{Test}} * 100[\%] \approx 28\%$$

This difference of 28 % can be regarded to be quite good, if we take into account, that the cross sections of the cylinders tested are not really an ideal circle, and also the laminate thicknesses are not exactly constant . That means, a little geometric imperfection, which would reduce the calculated buckling load, would bring it closer to the test result.
Due to the manufacturing process also some unknown laminate defficiencies like other fiber orientation angles, deviations in the material data, other fiber volume contents etc. could occur.
Of course all these imperfections and laminate defficiencies will reduce the buckling loads of the tested cylinders.

If we compare the MARC result of 15.89 kNm with the theoretical value of *15.63 kNm* , we get a very good conformity (only 2 promille difference).
Due to this good correspondance between the test result, the analytical value and the numerical calculations performed with the MARC FEM program, the validation of the used numerical tool has been shown.

The predicted mode shapes calculated in Ref. [9] with the FEM program STAGS for the cylinder CYL-1B with stacking-sequence -45° , +45° , 0° , 90° with t = 0.953 mm (see Table 3) are similar to the calculated ones determined with MARC, see Fig. 7.
Figure 16 shows these predicted mode shapes for two specimen CYL-1B and CYL-3A, see Ref. [9].

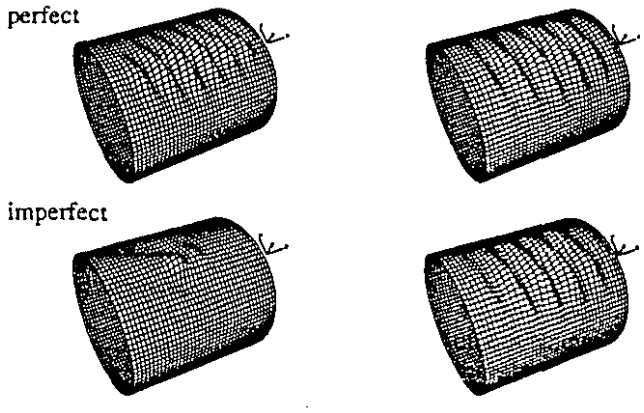

(a) CYL-1B, $[\mp 45/0/90]_S$ (b) CYL-3A, $[\mp 45/0_2]_S$

Fig. 16 : Predicted mode shapes for two specimen CYL-1B and CYL-3A, figure is taken from Ref. [9]).

3. FEM ANALYSIS OF A BELLOW-SHAPED SPRING USED FOR THE EC135 ARIS SYSTEM

For a metallic bellow shaped spring element of a hydro-mechanical isolator element as used for the EC135 - helicopter, a nonlinear FEM analysis was conducted.
This spring element - called primary bellow - is exposed to large displacements as well as high internal pressure caused by the internal fluid.

One aim of this analysis was the consideration of wall thickness variations along the bellow axis direction. Another target was to take into account the nonlinear material behaviour of the used material 17-4PH steel (US norm), which is same as the German 1.4548 - material.
For this material stress - strain curves are available from the manufacturer, and thus, the whole elastic and plastic material behaviour could be realised for the FEM analysis using the ' Finite Strain Plasticity '- capability of the MARC FEM-code.

Apart from the determination of stress distributions in the outer and inner bellow regions, also special attention had to be paid to the axial stiffness of this primary bellow. The value of this axial stiffness has a significant influence on the proper function of the complete ARIS-system as a fine tuned spring - damper - mass - system, see Ref. [12].

3.1 Description of the design

The ARIS is an Antiresonant Rotor Isolation System, which is based on a spring mass system and which works on the principle of hydraulic force transfer. It is mounted between main gear box and fuselage in order to avoid vibration induction from the main rotor into the fuselage. The main components of the ARIS are metallic bellows, which serve as a spring and in addition enclose the hydraulic liquid. Therefore the bellows are loaded by hydraulic pressure and by axial external forces.

Fig. 17 shows the main components of the EC135-ARIS system in a cross sectional view, whereas Fig. 18 explains the mechanical principle.

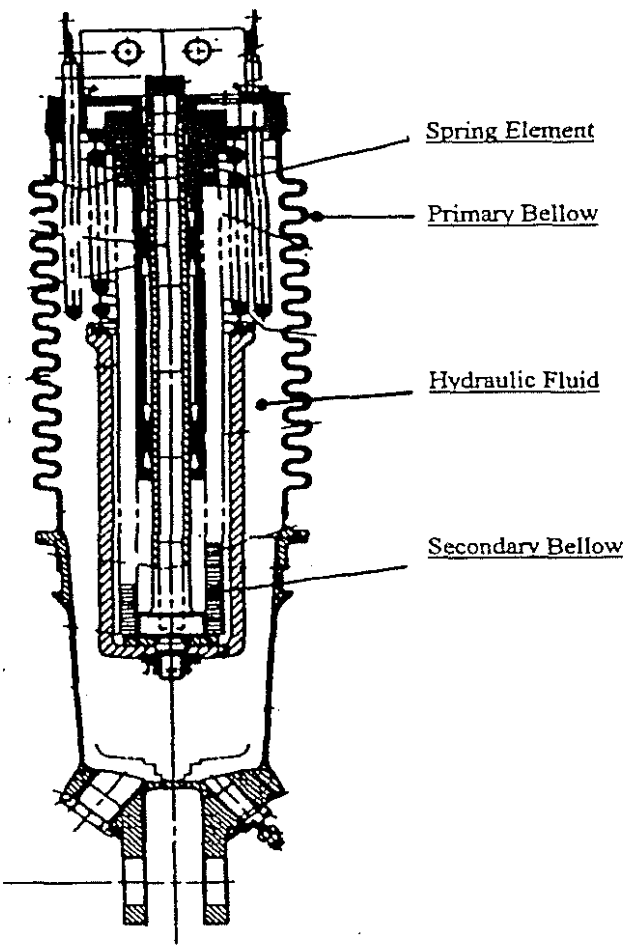

Fig. 17 : The main components of the ARIS-system as used for the EC135-P1/T1 helicopter.

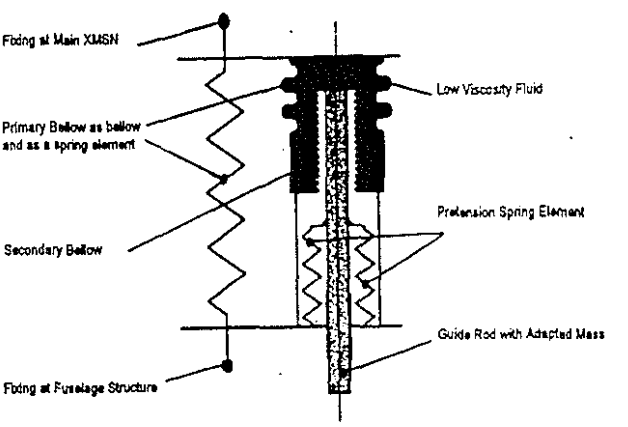

Fig. 18 : Mechanical Principle of the EC135-ARIS-system, figure is taken from Ref. [12].

3.2 Nonlinear Analysis with the FEM code MARC

For the primary bellow of the EC135 hydraulic ARIS system a nonlinear FEM analysis with MARC was conducted. With this tool not only high geometrically nonlinearities due to large deformations, but also plastic material behaviour can be taken into account. This analysis was conducted at the RWTH Aachen (see Ref. [12]) and ECD in Munich.

MARC has different tools for the consideration of elastic/plastic material behaviour. It is beyond the scope of this presentation, to deal with all the details. For more information please refer to the theory handbooks from MARC as given in Ref. [11].
Nevertheless, some basic informations will be given, in which way elastic/plastic material behaviour was considered in the analysis using the Ramberg-Osgood approach.

3.2.1 Basic numerical tools for elastic/plastic material behaviour

According to Ref. [15] the stress-strain diagram of metals without a yield plateau can very accurately be represented by means of the RAMBERG-OSGOOD - formula :

$$\varepsilon = \varepsilon_{Elastic} + \varepsilon_{Plastic}$$

$$\boxed{\varepsilon = \frac{\sigma}{E} + \left(\frac{\sigma}{B}\right)^{n}}$$

Here, E is the Young's modulus, and B and n are material constants.
The tangent modulus is then given by, see Ref. [15] :

$$E_t = \left(\frac{d\sigma}{d\varepsilon}\right) = \frac{E}{1 + n * \frac{E}{B} * \left(\frac{\sigma}{B}\right)^{(n-1)}}$$

The material 17-4PH assumed for the primary bellow has a stress-strain curve without a yield plateau, and the material constants B and n can be determined from the given curve for 17-4 PH stainless steel for condition H900 (special heat treatment) from tensile stress-strain curves as specified in the Military Standard Handbook MIL-HDBK-5C page 2-173. These data point out for condition H900 a value of n = 11 for the material constant of the Ramberg-Osgood material rule.

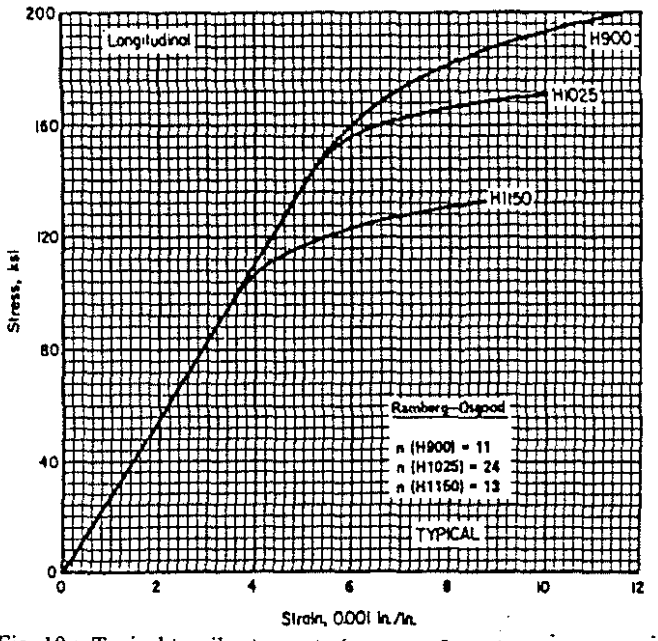

Fig. 19 : Typical tensile stress-strain curves from the Military Standard Handbook MIL-HDBK-5C page 2-173, for 17-4 PH stainless steel for different conditions (figure is taken from Ref. [16]).

There are two methods in order to specify the stress strain data for the FEM analysis with MARC.
In the first method, the workhardening slopes for uniaxial stress data as a change in stress per unit of plastic strain (see Fig. 20 above) and the plastic strain at which these slopes become effective (breakpoints).

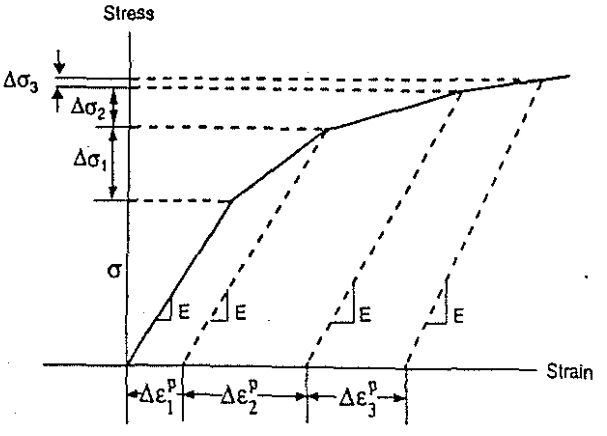

Fig. 20 : Workhardening Slopes, from Ref. [11].

The other method requires the input of a table of yield stress, plastic strain points. This option is flagged by adding the word DATA to the work hard statement in the FEM model.

The yield stress and the workhardening data must be compatible with the tools used for the analysis. If the LARGE DISP , UPDATE and FINITE options are used - as it is the case for our calculations for the primary bellow - the yield stress must be defined as a true or Cauchy stress, and the workhardening data with respect to logarithmic plastic strains.

These logarithmic plastic strains have to be used by the formula given in Ref. [11] and [12] :

$$\varepsilon_P^{\ *} = \log(1+\varepsilon-\frac{\sigma}{E})$$

3.2.2 Description of the FEM model

For the FEM calculations two different numerical models have been used. The first one consists of axisymmetric MARC shell elements type 89. These shell elements have 3 integration points (Gauss Points) and can be used for thick walled shell structures together with the AXISYMMETRIC option of MARC.
This tool allows the generation of a rotational symmetric structure. This allows to use much less elements compared to a 3D shell model, but can be used without difficulties only if the loads are also axisymmetric.
This is here the case for internal pressure and tension/compression loading.
If the condition for complete rotational symmetry is valid in geometry as well as loading, this advantage of a small model can be used successfully for the nonlinear analysis, since this Meridian-FEM-model consists of much less degrees of freedom. The model in circumferential direction will be automatically completed for the analysis by MARC using Fourier series.
Since the computation time depends quadratically from the degrees of freedom of the whole structure, the total time needed for the nonlinear analysis is much lower compared to the 3D model.

Fig 21 shows this Meridian FEM model also giving the definition of the coordinate system used to specify the boundary conditions. According to Ref. [11] X defines the direction parallel to the rotational axis, Y defines boundary conditions *in the radial direction and Z defines rotations* about an axis perpendicular to the x- y- plane.

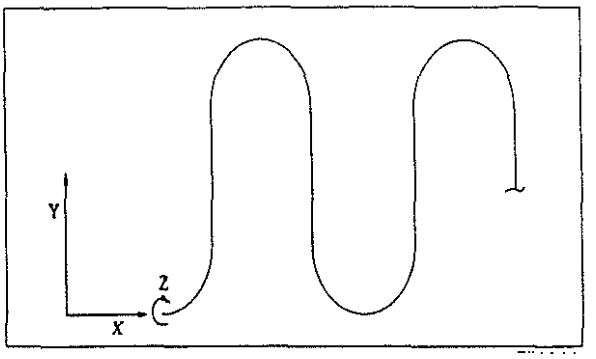

Fig 21: The Meridian-model, coordinates for the definition of boundary conditions.

In spite of all advantages of this Meridian-FEM-model also an analysis has been conducted for a 3D shell modell of the primary bellow. If this model comes to same results, the reliability of the nonlinear analysis would be increased. On the other hand, this 3D model using 4 node bilinear shell elements with transverse shear capability (MARC element typ 75) could be used if non-symmetrical loading should be considered.
In order to reduce time and storage space for the analysis, only 2 waves instead of 12 of the primary bellow had been modeled.

This 3D shell model is shown in Fig. 22 above.

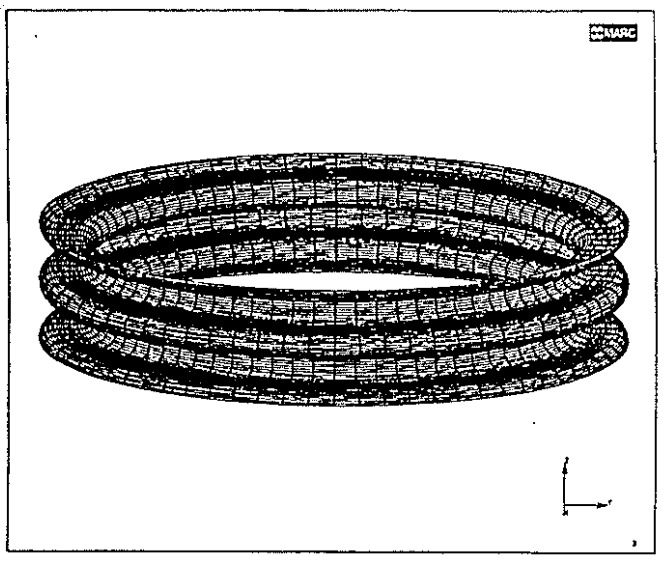

Fig. 22 : 3D shell elements typ 75 - FEM model,
(only 2 waves in meridian direction have been modeled).

For the nonlinear MARC analysis additionally following tools have been used (the MARC-keywords are given in capital letters) :

(a) FOLLOW FOR
This option is necessary because the stress analysis has to be conducted for a structure which is loaded by non-conservative loading as it is the case for internal pressure,

(b) LARGE DISP
Activates the non-linear stress analysis tools in MARC, which are necessary for the consideration of large deformations of the structure,

(c) UPDATE
The Updated Lagrange Procedure improves the results of the non-linear stress analysis and is necessary for taking into account the plastic material behaviour,

(d) FINITE
The Finite Strain Plasticity option is also necessary for the analysis with nonlinear material behaviour. The material properties (stress-strain curve) have to be defined as a table giving the Cauchy stresses (true stresses) related to logarithmic plastic strains (see chapter before).

Geometry

The geometrical data for the primary bellow are specified by the drawing number L 633M2002 213 from Eurocopter Deutschland GmbH. The variation of the wall-thicknesses have been considered in the FEM model using the thickness measurements from the manufacturer Witzenmann.
Thus for both FEM models - the meridian- and the 3D-shell model - the real distribution of wall-thicknesses have been taken into account in order to calculate the axial stiffness accurately.

Matertial Plasticity

According to Ref. [12], the plastic material behaviour was integrated in the FEM model using the relation:

$$\varepsilon_P^{\,*} = \log\left\{1+\left[\frac{\sigma_{0,7}}{E}\left(\frac{\sigma}{\sigma_{0,7}}-\frac{3}{7}\left(\frac{\sigma}{\sigma_{0,7}}\right)^{N}\right)\right]-\left[\frac{\sigma}{E}\right]\right\}$$

Here in the first term [....] , the total strain according to Ramberg-Osgood is calculated, and then reduced by the second term [....] representing the elastic part.

Some important features of the meridian FEM model should be given in the following as extracted parts of the complete MARC input file:

```
title    EC135-ARIS primary bellow
title    Meridianmodel
title    3 Node thick shell elements typ 89
title    elastic / plastic material 1.4548.6
title    Ramberg-Osgood material rule
sizing          1000000  112  225  675
elements        89
large disp
update
finite
follow for  1
all points
dist loads  1   112
shell sect      5
setname         4
end
solver
    0       0       0
optimize            9
```

connectivity

```
   1  89     1    105    2
   2  89     2    106    3
   3  89     3    107    4
. . . . . .
  etc.
. . . . . .
```

coordinates

```
3     225
1     5.94000+1     5.09958+1     0.00000+0
. . . . . .
```

etc. global x- y- z-coordinates of Nodes

```
. . . . . .
```

isotropic

```
Ivon mises isotropic          0       0
1.96000+5     3.00000-1       7.86000-3 .
1          to          112
```

work hard data

```
    101         0         1         0
6.20700000e+02          0.00000000e+00
6.30493000e+02          3.59049549e-07
. . . . . .
```

etc. Table for Cauchy stress and logarithmic plastc strain

```
. . . . . .
```

geometry

```
 1.63000+0 0.00000+0 0.00000+0 0.00000+0 0.00000+0
      41        42        75        76        77        78
 1.62000+0 0.00000+0 0.00000+0 0.00000+0 0.00000+0
      43        74        79       110
 1.60000+0 0.00000+0 0.00000+0 0.00000+0 0.00000+0
      44        73        80       109
 1.58000+0 0.00000+0 0.00000+0 0.00000+0 0.00000+0
      45        72        81       108
 1.55000+0 0.00000+0 0.00000+0 0.00000+0 0.00000+0
      46        71        82       107
 1.53000+0 0.00000+0 0.00000+0 0.00000+0 0.00000+0
      47        70        83       106
 1.49000+0 0.00000+0 0.00000+0 0.00000+0 0.00000+0
      48        69        84       105
 1.46000+0 0.00000+0 0.00000+0 0.00000+0 0.00000+0
      49        68        85       104
 1.42000+0 0.00000+0 0.00000+0 0.00000+0 0.00000+0
  1         2         3         4         5         6         7
 10        11        12        13        14        15        16
 19        20        21        22        23        24        25
 28        29        30        31        32        33        34
 37        38        39        40        50        51        52
 55        56        57        58        59        60        61
 64        65        66        67        86        87        88
 91        92        93        94        95        96        97
100       101       102       103
fixed disp

 0.00000+0
    3
      45
 0.00000+0 0.00000+0
    1    3
     216
point load

-5.20480+3 0.00000+0 0.00000+0
      45
```

```
dist loads

    0-7.50000-1
       1        to       112
no print
post
   13   16   17    1    0   19   20    0    1    0    6
  311    1
  311    3
  311    5
   17    1
   17    3
   17    5
  127    1
  127    3
  127    5
   27    1
   27    3
   27    5
   20
end option
$...................
```

$.....start of loadcase lcase1

```
control
99999   10    0    0    0    1    0    0    1    0
 1.00000-1 0.00000+0 0.00000+0 0.00000+0 0.00000+0 0.00000+0
auto time
 2.00000-2 1.00000+0 0.00000+0 1.00000+0 5.00000-1 1.10000+0
0.00000+0
disp change
    0    0    1

-8.33300-1 0.00000+0
    1    3
      45
 0.00000+0 0.00000+0
    1    3
     216
point load    0

 4.15290+3 0.00000+0 0.00000+0
      45
dist loads    0

    0 5.98430-1
       1        to       112
continue
$....end of loadcase lcase1
$...................
```

3.2.3 FEM results

For a given axial displacement of + 10 mm in tension and - 10 mm in compression the results for the two used FEM models are given in comparison in Fig. 23 above for a constant wall thickness of t = 1.45 mm , see Ref. [12].
The calculated axial stiffnesses, equivalent elastic strains and the equivalent Von-Mises stresses are in very good correlation between both models.
For both analyses the same assumptions with respect to geometry, boundary conditions, material data and wall thicknesses have been used.
We can see, that the more effective meridian model comes to same results in less computation time then the 3D-shell model.

	Variable	Schalenmodell		Meridianmodell	
		Knoten		Knoten	
f_{ax} = -10 mm	k_{ax}		3688 N/mm		3686 N/mm
	$\sigma_{V\,(equival.\,Von\text{-}Mises\,stress)}$	1, 4033, 8065	202 N/mm²	1, 113, 225	202 N/mm²
		2017, 6049	211 N/mm²	57, 169	211 N/mm²
	$\varepsilon_{(equivalent\,elastic\,strain)}$	1, 4033, 8065	0,85%	1, 113, 225	0,88%
		2017, 6049	1,02%	57, 169	1,02%
f_{ax} = +10 mm	k_{ax}		3822 N/mm		3820 N/mm
	$\sigma_{V\,(equival.\,Von\text{-}Mises\,stress)}$	1, 4033, 8065	233 N/mm²	1, 113, 225	233 N/mm²
		2017, 6049	239 N/mm²	57, 169	240 N/mm²
	$\varepsilon_{(equivalent\,elastic\,strain)}$	1, 4033, 8065	0,85%	1, 113, 225	0,88%
		2017, 6049	1,02%	57, 169	1,02%

Fig. 23 : Results for the two different FEM models in comparison, taken from Ref. [12].

The results of the nonlinear elastic/plastic analysis are given for the axial stiffnesses in Fig.24 for the model with different shell thicknesses as measured by the manufacturer (thickness t changes in meridian direction between 1.42 and 1.63 mm).

We can see, that for little axial displacements fax [mm] no difference occurs between an elastic analysis in comparison to the nonlinear plastic analysis. This is not true for higher loading in tension or compression corresponding to larger axial deformations.
In this region at nearly + 6 mm in tension and - 6 mm in compression the axial stiffness or spring konstant C of the primary bellow becomes more and more non-linear.
For displacements less then +- 6 mm the primary bellow can be regarded to be a linear spring element.

The MARC results are given in the lower curve (dashed line for the pure elastic analyses full line for plastic analyses), whereas the upper curve has been determined by means of a special shell calculation program, which has been developed at the RWTH Aachen acc. to Ref. [12].

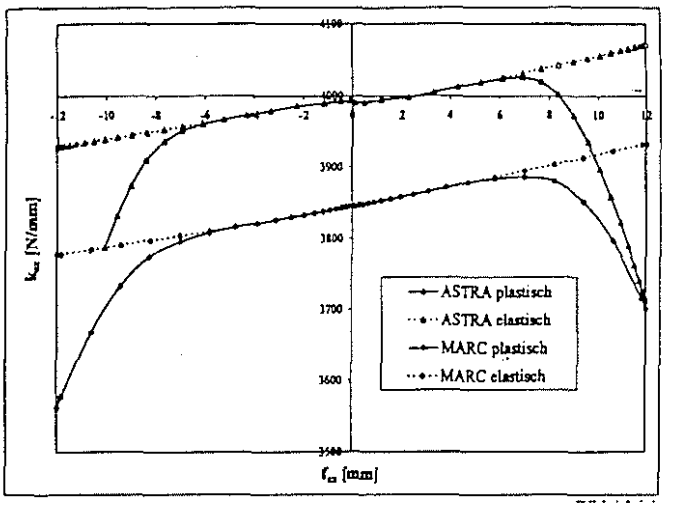

Fig. 24 : Axial stiffness for elastic and plastic analysis in comparison, taken from Ref. [12].

The FEM results for the stress analysis are given in Fig. 25 for the direct stresses over the radians length in [mm] for a given axial total displacement of + 12 mm in tension. The corresponding Von-Mises stresses are shown in Fig. 26.
Taking into account the plastic material behaviour reduces the maximum equivalent direct stress to a value of nearly 1400 MPa.

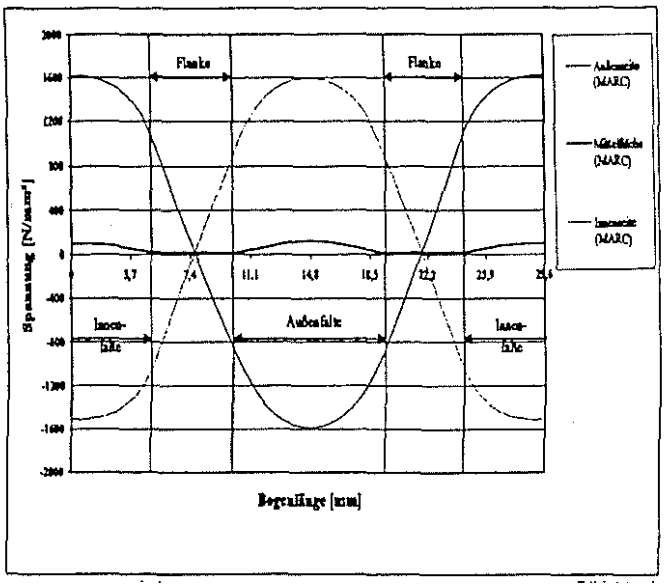

Fig. 25: *Direct stresses over radians length for* 12 mm total axial tension displacement, figure is taken from Ref. [12].

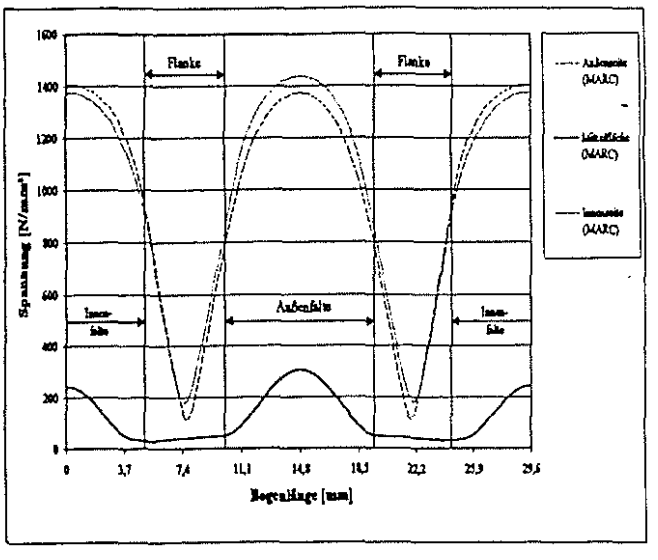

Fig. 26: Von-Mises stresses over radians length for 12 mm total axial tension displacement, figure is taken from Ref. [12].

3.3 Validation of the numerical tools by comparison with test results

At Eurocopter as well as by the manufacturer Witzenmann, tests were conducted with the same primary bellows as the calculated ones, and the axial stiffnesses in tension and compression with and without internal pressure loading were determined.

These measurements have led to stiffness values between

$$C \approx 3870 \text{ and } 3960 \text{ N/mm}.$$

The comparison of these values with the calculated value by MARC as given in Fig.24 of nearly 3840 N/mm , shows a very good conformity, if we take into account the scatter of the material data (Young's modulus) and the wall thicknesses of the tested bellows.

Since there is a good correspondance in calculated and measured stiffnesses, also the stresses and strains calculated by the numerical tool MARC could be validated.

REFERENCES

[1] Dr. Michelis, P.
"Design and Validation of Imperfection-Tolerant Laminated Shell Structures",
Brite-Euram Project 7550, DEVILS,
Contract No. BRE2-CT94-0962,
Detailed Description of Tasks for the Workprogram,
IMMG Athen , Greece,
December 1996

[2] Dr. Bansemir, H., Müller, R.
"The EC135 - Applied Advanced Technology",
AHS 53rd, Annual Forum and Technology Display,
April 29 - May 1, 1997,
Virginia Beach, Virginia, USA

[3] Schröder, P.
"Über das Beulverhalten querkraft-belasteter Kreiszylinder",
Deutsche Luft- und Raumfahrt,
Forschungsbericht 73-62,
Deutsche Forschungs- und Versuchsanstalt für Luft- und Raumfahrt, Institut für Flugzeugbau,
Braunschweig , 1973

[4] Prof. Dr.-Ing. habil. Hampe, E.
" Stabilität rotationssymmetrischer Flächentragwerke ",
Verlag von Wilhelm Ernst & Sohn ,
Berlin, München,
1983

[5] Gergely,P., Bongers,B.
" ECD Contribution to Task 4.2 - Preliminary Design Guidelines ", Brite-Euram Project 7550, DEVILS, Report No. WP01.DR / ECD(4) ,
Eurocopter Deutschland GmbH , March 12 1997

[6] Gergely,P.
"ECD contribution to Validation of numerical/analytical models within the framework of Subtask 3.2 and 3.3 for casestudy 1 & 2",
Report No. WP04.DR/ECD(3) ,Februar 28, 1997,
ECD GmbH, Ottobrunn, Germany

[7] Gergely,P.
"Buckling Analysis of a Transverse Loaded Astralon Cylinder using the FEM Code MARC K6.2",
Report No. ECD-0080-97-PUB , ECD GmbH,
Ottobrunn, Germany, for the MARC Users Meeting held in Munich Germany, October 15-16, 1997

[8] Dr. Chryssanthopoulos, M.K. , et al
" First Draft of Design Guidelines for Composite Shell Structures „
Brite-Euram Project 7550, DEVILS,
Contract No. BRE2-CT94-0962,
Report No. WP02.DR/IMP(4) , March 27, 1997,
Imperial College, London, UK

[9] Fuchs, H. P.,Starnes, J. H.,Hyer, M. W.
" Prebuckling and collapse response of thin-walled composite Cylinders subjected to Bending Loads ",
Virginia Polytechnic Institute and State University, Blacksburg, Virginia 24061-0219, USA, and NASA Langley Research Center, Hampton ,
Virginia 23681-0001, USA

[10] Huyan, X.,Simitses, G.J.,Tabiei, A.
" Nonlinear Analysis of Imperfect Metallic and Laminated Cylinders Under Bending Loads ",
University of Cincinnati, Cincinnati,
Ohio 45221-0070,
AIAA JOURNAL Vol. 34 , No. 11 ,
November 1996,

[11] MARC
Users Manuals,
Volumes A, B, C

[12] Kämpchen,M.
" Statische und dynamische Festigkeitsuntersuchungen zu Metallbälgen für Hubschrauberschwingungsisolationssysteme ", Diplomarbeit am Institut für Leichtbau der RWTH Aachen,
Univ.-Prof. Dr. Ing. H.-G. Reimerdes
DA-98-1 , Aachen , Germany, März 1998

[13] Military Handbook , composite structures
MIL-HDBK-17

[14] Luftfahrt-Tauglichkeits-Forderungen, Angaben zur Anerkennung von Dimensionierungskennwerten für Verbundwerkstoffe aus faserverstärkten Kunststoffen,
LTF 9330-302 , Bundesamt für Wehrtechnik und Beschaffung, Juni 1986

[15] Massonnet,Ch., Olszak, W., Phillips, A.
Plasticity in Structural Engineering Fundamentals and Applications ,
International Centre for Mechanical Sciences,
Courses and Lectures - No. 241 ,
Springer Verlag , Wien New York

[16] Military Handbook , Metallic Parts
MIL-HDBK-5C ,
dated 1 December 1979